Nuclear Inst. and Methods in Physics Research, A 891 (2018) 42–52

Contents lists available at ScienceDirect

Nuclear Inst. and Methods in Physics Research, A

journal homepage: www.elsevier.com/locate/nima

Precise rise and decay time measurements of inorganic scintillators by means of X-ray and 511 keV excitation

S. Gundacker [a,b,*], R.M. Turtos [a,b], E. Auffray [b], P. Lecoq [b]

[a] UniMIB, Piazza dell'Ateneo Nuovo, 1 - 20126, Milano, Italy
[b] CERN, 1211 Geneve 23, Switzerland

ARTICLE INFO

Keywords:
Scintillation emission kinematics
Scintillation rise time
Fast timing
10 ps TOF-PET
Inorganic scintillator

ABSTRACT

The emergence of new solid-state avalanche photodetectors, e.g. SiPMs, with unprecedented timing capabilities opens new ways to profit from ultrafast and prompt photon emission in scintillators. In time of flight positron emission tomography (TOF-PET) and high energy timing detectors based on scintillators the ultimate coincidence time resolution (CTR) achievable is proportional to the square root of the scintillation rise time, decay time and the reciprocal light yield, $CTR \propto \sqrt{\tau_r \tau_d / LY}$. Hence, the precise study of light emission in the very first tens of picoseconds is indispensable to understand time resolution limitations imposed by the scintillator. We developed a time correlated single photon counting setup having a Gaussian impulse response function (IRF) of 63ps sigma, allowing to precisely measure the scintillation rise time of various materials with 511keV excitation. In L(Y)SO:Ce we found two rise time components, the first below the resolution of our setup <10 ps and a second component being ~380 ps. Co-doping with Ca^{2+} completely suppresses the slow rise component leading to a very fast initial scintillation emission with a rise time of <10ps. A very similar behavior is observed in LGSO:Ce crystals. The results are further confirmed by complementary measurements using a streak-camera system with pulsed X-ray excitation and additional 511 keV excited measurements of Mg^{2+} co-doped LuAG:Ce, YAG:Ce and GAGG:Ce samples.

1. Introduction

There is an increasing demand for fast timing in high energy physics and molecular positron emission tomography (PET) imaging. In high energy physics (HEP) the precise time tagging of minimum ionizing particles (MIPs) improves the vertex reconstruction in detectors for future high luminosity accelerators. One way to build such detectors is to use a scintillating crystal coupled to a photodetector, e.g. silicon photomultiplier (SiPM). HEP applications for example demand a timing resolution of <20 ps with the constraint of small crystal dimensions of about 3 mm in thickness, leading to a low energy deposit of the detected MIP in the crystal (~3 MeV) and hence photostatistics being the dominant factor in the best achievable time resolution. In PET, time of flight (TOF) is already well established as an indispensable modality in next generation machines. Future efforts will further go towards highest time resolution to ultimately reach 10 ps in TOF-PET, corresponding to 1.5 mm resolution along the line of response (LOR). This additional timing information will solve the inverse problem which then allows for new PET geometries as a full 360° coverage is not a necessity anymore. Another advantage of 10 ps in PET will be a more than hundred-fold sensitivity gain which most likely will change the view on PET in the clinical routine, being able to allow for lowest dose PET/MR images and/or much faster scanning times. Such high time resolutions will further fundamentally change how PET images will be reconstructed giving new opportunities in image quantification, attenuation and motion correction. The standard TOF-PET module is built of a scintillating crystal readout by a photodetector (SiPM). In such a system the ultimate time resolution is as well given by the scintillation emission time structure, i.e. the rise time τ_r and decay time τ_d. If only scintillation statistics is considered, the coincidence time resolution (CTR) of a TOF-PET detector would be directly proportional to the square root of the scintillation rise time (τ_r), as shown in Eq. (1). The factor 2.18 is a consequence of determining the time variance of the first scintillation photon emitted and includes the transformation into FWHM of the standard deviation [1].

$$CTR_{1^{st}} = 2.18 \cdot \sqrt{\frac{\tau_r \cdot \tau_d}{n'}}. \quad (1)$$

Eq. (1) contains as well the scintillation decay time τ_d and the number of photons detected by the photodetector n' and is strictly valid

* Corresponding author at: CERN, 1211 Geneve 23, Switzerland.
E-mail address: stefan.gundacker@cern.ch (S. Gundacker).

https://doi.org/10.1016/j.nima.2018.02.074
Received 8 November 2017; Received in revised form 25 January 2018; Accepted 15 February 2018
Available online 23 February 2018

Table 1
Samples for which the scintillation emission rate was measured. Co-doping stated was available in addition to normal Ce doping. Sample dimensions are $2 \times 2 \times 10$ mm^3 except for LuAG:Pr with $2 \times 2 \times 8$ mm^3.

Composition	Doping	Co-doping	Producer
LSO	Ce	Ca (0.2% or 0.4%)	Agile
LYSO	Ce	–	CPI, Epic
LGSO	Ce	–	Hitachi
LFS	Ce	–	Zecotek
GAGG	Ce	–	Furukawa
GAGG	Ce	Mg (0.1%)	C&A
LuAG	Ce	Mg (0.3%)	details see [5]
YAG	Ce	Mg (0.3%)	details see [5]
LuAG	Pr	–	A. Petrosyan

for the limit $\tau_d \ll \tau_r \cdot n'$, which is true for typical LSO crystals. It already gives a good estimate of the limits in terms of time resolution considering only the scintillation process itself. For an intrinsic light yield of 20 500 photons per 511 keV, a rise time of 70 ps and a decay time of 40 ns, the $CTR_{1st} = 25$ ps FWHM. Lowering the rise time to 20 ps and the decay time to 30 ns would lower this value to $CTR_{1st} = 12$ ps FWHM. In the case of a zero rise time ($\tau_r = 0$) Eq. (1) would simply become $CTR = 3.33 \cdot \tau_d / n'$ shown by Post and Schiff in 1950 [2] with the $CTR_{1st} = 5$ ps for 20 500 photons detected and a 30 ns decay time constant. These calculations show that achieving a time resolution of 10 ps FWHM in coincidence calls for the need to look at the scintillation rise time and more in general at the production of prompt photons at the beginning of the scintillation process [3,4].

This paper will present precise rise time measurements for different ortho-oxysilicates and garnet scintillators comparing X-ray and 511 keV excitation. It basically follows the philosophy of one of our previous publications [4], presenting more precise measurements with higher acquisition statistics and compares results to X-ray exited measurements done with a streak-camera. In Section 2 the measurement setups and data analysis will be described followed by the presentation of the results in Section 3. Section 4 will present discussions on the quality of fit for the obtained decay time values and investigates the bias of prompt photons, e.g. Cherenkov emission, to the performed scintillation rise time fits. Finally we will give a short outlook on how a fast scintillation emission and especially prompt photons can help to achieve highest time resolution in TOF-PET and in high energy physics.

2. Materials and methods

2.1. Samples

We measured the scintillation emission kinematics of different oxides doped with Cerium, i.e. LSO:Ce, LYSO:Ce, LGSO:Ce and LFS:Ce, from which LSO:Ce was as well co-doped with 0.2% or 0.4% Calcium. In order to study the effect of co-doping with divalent ions more in depth we as well measured garnet crystals, i.e. GAGG, LuAG and YAG, doped with Cerium and all additionally co-doped with Magnesium. All of these samples have the same dimensions of $2 \times 2 \times 10$ mm^3. Further we used one LuAG:Pr sample to study the effect of prompt photon production with 511 keV excitation in comparison to X-ray excitation with a mean energy of 15 keV. Table 1 summarizes the used samples for these studies.

2.2. 511 keV excitation: TCSPC setup

To measure the scintillation emission we used a modified time correlated single photon counting (TCSPC) setup in which we as well monitor the energy deposit in the crystal under test, as can be seen in Fig. 1. The start detector consists of a $2 \times 2 \times 5$ mm^3 LSO:Ce co-doped with 0.4%Ca crystal covered in Spectralon and mounted to a S10931-050P MPPC from Hamamtsu with optical glue [4]. We measured the time performance of the start detector in a coincidence setup and determined its resolving time to 107 ps FWHM [6]. As stop detector a single photon avalanche diode (SPAD) with $(50 \times 50)\mu m^2$ from ID-Quantique (IDQ) ID100-50 was used. This SPAD was specially selected for low dark noise and additionally cooled with a Peltier element to reduce the dark noise even further to values of 20 Hz. The time resolution of the stop detector we measured to 94 ps FWHM using a picosecond-laser with 405 nm wavelength [4]. Combining the resolving times of the start and stop detector gives the impulse response function (IRF) to be Gaussian with a sigma of 60 ps (or 142 ps FWHM). This approach is valid, as the photon transfer time spread in the crystal under test is in the range of 10 ps (only a small volume of around $3 \times 1.5 \times 2$ mm^3 is seen by the stop-detector) and, hence, almost negligible. However, in order to determine the IRF finally and in a precise way we used Cherenkov photons produced in an undoped LuAG scintillator. The obtained IRF was Gaussian with a sigma of 63 ± 3 ps, which is in accordance to the separate time resolutions of start and stop detectors measured. A further explicit description of the setup including the exact determination of the IRF can be found in [4].

The measured scintillation emission rate is a product of the convolution of the intrinsic emission rate with the impulse response function (IRF) of the measurement system. The IRF with $\sigma_{IRF} = 63 \pm 3$ ps is stated in Eq. (2), with Δ_M a possible electronic delay. We model the intrinsic scintillation emission with a multi exponential structure with several rise ($\tau_{r,i}$) and decay ($\tau_{d,i}$) times with the start of the scintillation process at time θ, as can be seen in Eq. (3). The function $\Theta(t)$ is the Heaviside function with $\Theta(t<0)=0$, $\Theta(t=0)=0.5$ and $\Theta(t>0)=1$. The relative weights of the different components are defined by Eq. (4), however most of the times one or two weights are sufficient, e.g. in the case of a one component fit $\rho = 1$, and for a two component fit $\rho_1 = R$ and $\rho_2 = 1-R$ with R between 0 and 1. In the analysis we as well include the possibility of prompt photon emission (e.g. Cherenkov or hot-intraband luminescence) at the onset of the scintillation with amplitude $Camp$, as can be seen in Eq. (5). Here $\delta(\theta)$ is the Dirac-delta function, implying that prompt photons are modeled to be produced all the same time. The convolution with the IRF is stated in Eq. (6) and solved analytically in Eq. (7). The prompt photon emission appears at the onset of the scintillation process as the IRF with amplitude "Camp".

$$g(t) = \frac{1}{\sigma_{IRF}\sqrt{2\pi}} \exp\left[-\frac{(t-\Delta_M)^2}{2(\sigma_{IRF})^2}\right] \tag{2}$$

$$f(t|\theta) = \Theta(t-\theta) \sum_{i=1}^{N} \frac{e^{-(t-\theta)/\tau_{d,i}} - e^{-(t-\theta)/\tau_{r,i}}}{\tau_{d,i} - \tau_{r,i}} \cdot \rho_i \tag{3}$$

$$R_i = \frac{\rho_i}{\sum_{i=1}^{N} \rho_i} \tag{4}$$

$$f^p(t|\theta) = f(t|\theta) + Camp \cdot \delta(\theta) \tag{5}$$

$$\begin{aligned} f_g^p(t|\theta) &= f^p(t|\theta) * g(t) \\ &= \int_{-\infty}^{\infty} f^p(t'|\theta)\, g(t-t')dt' \end{aligned} \tag{6}$$

$$\begin{aligned} f_g^p(t|\theta) = &\sum_{i=1}^{N} \frac{\rho_i}{2(\tau_{d,i}-\tau_{r,i})} \exp\left(\frac{2\tau_{d,i}(\Delta_M+\theta-t)+\sigma_{IRF}^2}{2\tau_{d,i}^2}\right) \\ &\cdot \left(1 - erf\left[\frac{\tau_{d,i}(\Delta_M+\theta-t)+\sigma_{IRF}^2}{\sqrt{2}\,\sigma_{IRF}\,\tau_{d,i}}\right]\right) \\ &- \sum_{i=1}^{N} \frac{\rho_i}{2(\tau_{d,i}-\tau_{r,i})} \exp\left(\frac{2\tau_{r,i}(\Delta_M+\theta-t)+\sigma_{IRF}^2}{2\tau_{r,i}^2}\right) \\ &\cdot \left(1 - erf\left[\frac{\tau_{r,i}(\Delta_M+\theta-t)+\sigma_{IRF}^2}{\sqrt{2}\,\sigma_{IRF}\,\tau_{r,i}}\right]\right) \\ &+ \frac{Camp}{\sqrt{2\pi}\sigma_{IRF}} \exp\left[-\frac{(t-\theta-\Delta_M)^2}{2(\sigma_{IRF})^2}\right]. \end{aligned} \tag{7}$$

In the analysis Eq. (7) is fitted to the measured data by means of χ^2 minimization (Eq. (8)), where i represents the ith bin with a typical

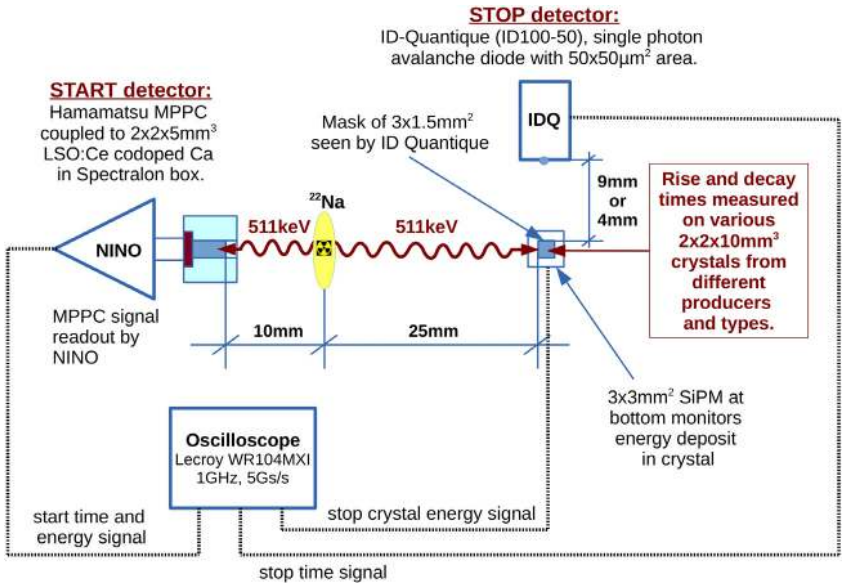

Fig. 1. Time correlated single photon counting setup used to measure the intrinsic rise- and decay-times of the inorganic scintillator samples.

width of 20 ps for the rise time fits and 0.2 ns for the decay time fits. Prior to fitting the background is evaluated and removed from the data followed by a normalization to the area. In the fit procedure we first determined the decay times not considering the rise time (set to zero). For L(Y,G)SO this is justified, as the slowest rise time is ~50 times faster as the fastest decay time observed. For crystals with longer rise times, e.g. GAGG:Ce, we first obtained the decay times including the fit of the rise time. Following we fixed the decay times and fitted the rise times again with higher precision.

$$\chi^2 = \frac{1}{N_{bins}} \sum_{i=1}^{N_{bins}} \frac{\left[\left(f_{data}\right)_i - \left(f_g^p\right)_i\right]^2}{\left(f_g^p\right)_i}. \quad (8)$$

In order to test this fitting procedure we generated via Monte Carlo simulations the measured data including background events with defined rise and decay time parameters. It was seen that the χ^2 weighting with f_g^p is not necessarily the best choice for the decay time fits, due to the presence of background events, which give a bias of the fit for long tails with low counts. We concluded that a square root weighting of χ^2 with $\sqrt{f_g^p}$ is more suitable for fitting decay times, especially in view of the best achievable timing with scintillators in e.g. time of flight positron emission tomography or high energy physics. In these cases the first nanoseconds of emission with higher amplitude are the most important and should therefore be weighted stronger as compared to baseline noise in the tail of the emission which is weighted less. We therefore resort to Eq. (9) for evaluating the scintillation decay times, whereas using the standard expression (8) for the rise time fits. However, if stating χ^2 values as a gauge for the goodness of fit we always use the standard expression given by Eq. (8), if not mentioned otherwise. The described fit-algorithm is able to determine the scintillation starting point (θ) and the rise time values independently, which was verified with our Monte Carlo simulations.

$$\chi^2 = \frac{1}{N_{bins}} \sum_{i=1}^{N_{bins}} \frac{\left[\left(f_{data}\right)_i - \left(f_g^p\right)_i\right]^2}{\sqrt{\left(f_g^p\right)_i}}. \quad (9)$$

2.3. X-ray excitation: streak camera

The schematics of the experimental setup used to measure the time-resolved X-ray excited emission is shown in Fig. 2, where the spectral time resolution is modulated by a system of horizontal and vertical slits. The time resolution of the camera under femtosecond laser excitation is ~18 ps FWHM and the repetition rate can go up to 4 MHz. Pulsed X-rays with energies up to 40 keV are triggered by a picosecond diode laser PiLAS operating at a wavelength of 372 nm. Samples are mounted few millimeters in front of the window of the Hamamatsu N5084 X-ray tube. Emitted radioluminescent light is spectrally dispersed by a 50 g/mm, 150 g/mm or 300 g/mm grating in a 2300 i spectrometer from Princeton Instruments and registered by a ~200 µm thin photocathode. The resulting photoelectrons are swept in the C10910 Hamamatsu streak camera tube and detected by a CCD with prior amplification in a photomultiplying microchannel-plate (MCP). The streak camera is operated in single photon counting mode using maximum MCP gain and setting the CCD threshold well above its noise floor, which has the advantage that thermal noise only arises from the photocathode and not the CCD.

A delay generator (represented by the clock in Fig. 2) provides the trigger signal for the laser and the streak camera sweeping unit. The dynamic range is adjustable from a 1 ns to 1 ms window, however, the number of bins is fixed at a value of 508 given by the CCD, e.g. for a 1 ns gate the bin width is 2 ps whereas for a 1 ms gate the bin width is 2 ns.

In order to determine the IRF of the whole acquisition system we measured the temporal profile of the laser under the exact same measurement settings as used for the actual measurements with crystals, i.e. sweeping range, optical path and photocathode slit aperture. Possible multiple reflections within the crystal are considered by measuring the laser light scattered in an undoped LuAG crystal positioned in front of the X-ray tube window. It should be noted that due to the low X-ray intensity the photocathode slit aperture has to be opened in order to improve the signal-to-noise ratio, which consequently deteriorates the IRF. For example, using a 100 µm slit aperture and a 5 ns sweeping range the laser shape is a Gaussian with 129 ps FWHM that has to be convolved with the asymmetric X-ray tube time response in order to obtain the complete IRF. Hence, the determination of the X-ray tube time profile is essential for the full characterization of the IRF. Experimental data with a N5084 X-ray tube excited by a femtosecond laser was taken using a C5680 X-ray streak camera which has a gold photocathode being able to directly convert X-rays in photoelectrons [7]. Results can be seen in Fig. 3, which shows the IRF of a N5084 X-ray tube. The simplest approach is to build the time response of the X-ray tube as an analytic function with a mono-exponential rise and decay component convolved with a Gaussian, as can be seen in Fig. 3 and expressed by Eq. (10) with

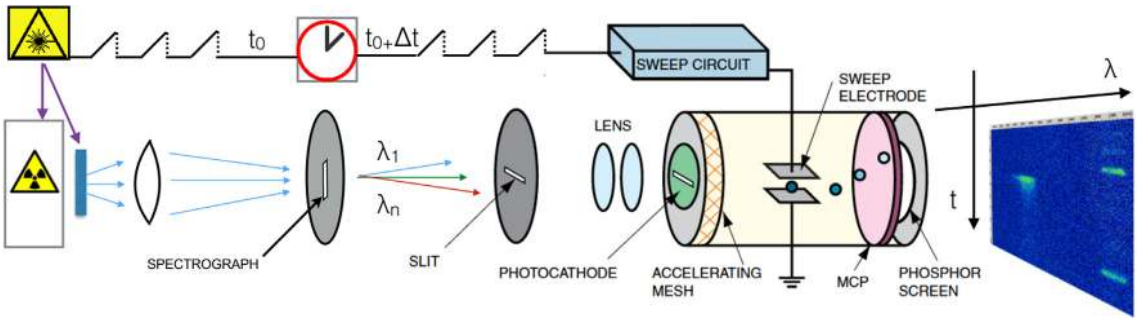

Fig. 2. Schematic view of the Streak camera setup. The X-ray tube with a maximum resulting energy of ~40 keV is driven by a PiLAS picosecond laser. The focused scintillation light is spectrally time resolved by the streak camera and analyzed by a PC.

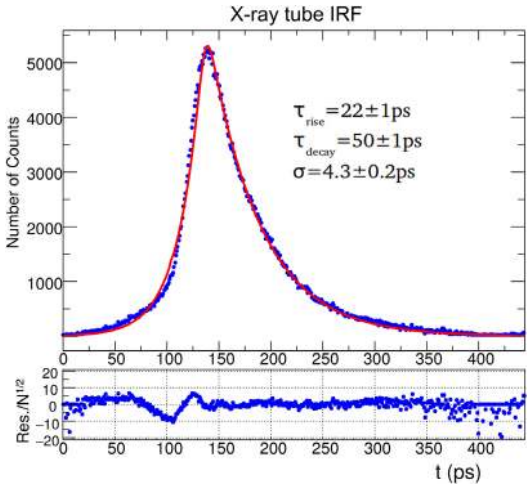

Fig. 3. Time response of the X-ray tube as measured by Hamamatsu using a X-ray streak camera in a 440 ps gate. The data is fitted to a monoexponential rise and decay model convolved with a Gaussian.

$\tau_r^X = 22,4$ ps, $\tau_d^X = 49.7$ ps and sigma $\sigma = 4.3$ ps.

$$IRF^{X-ray\ tube}(t) = \frac{1}{\tau_r^X + \tau_d^X}\left[\exp\left(\frac{t-\theta}{\tau_r^X}\right)\Theta(\theta - t)\ \ldots + \exp\left(\frac{\theta - t}{\tau_d^X}\right)\Theta(t-\theta)\right]\ \ldots \otimes \frac{1}{\sigma\sqrt{2\pi}}\exp\left[-\frac{(t-\Delta_M)^2}{2(\sigma)^2}\right]. \quad (10)$$

As already mentioned, the complete IRF of the streak camera system is the X-ray tube response as described by Eq. (10) convolved with the separately measured time profile of the laser plus streak camera including additional time smearing in the crystal caused by light reflection. More details on the determination of the complete IRF including a full calibration of the streak camera, e.g. background calibration, can be found in [8] on page 94 ff.

Since the streak camera IRF is rather complex and not a simple Gaussian the rise time fits for the X-ray excited data is performed numerically, however, with the same procedure described in the previous section. The convolution was done using a fast Fourier transformation using the corresponding probability density functions (PDFs). Parameter errors are calculated using the MINOS algorithm which has been designed to calculate the correct errors in all cases, especially when the functions are nonlinear. The theory underlying the non-parabolic log-likelihood method used is described in [9] (pp. 204–205).

3. Results

3.1. Oxides with X-ray excitation

Fig. 4 shows the comparison of fitting with a single or double exponential rise time for a X-ray excited LYSO:Ce scintillator from the producer CPI. It can be seen that a single rise time leads to a value of $\tau_r = 82$ ps and a χ^2 of 1.43, with a pronounced peak in the residual, to be seen on the left hand side in Fig. 4. The two component rise time fit shows for the first component $\tau_{r1} = 0$ ps with an abundance $R_1 = 82\%$ and for the second component $\tau_{r2} = 276$ ps with an abundance of $R_2 = 18\%$, to be seen on the right hand side of Fig. 4. The χ^2 calculated for the double rise time fit is 1.1, which constitutes a significant improvement (about 5 sigma) in the quality of fit as compared to the single exponential component fit.

Table 2 summarizes the obtained intrinsic scintillation rise times for different measured scintillator compositions and dopings measured with X-ray excitation. It can be seen that Ca^{2+} co-doped compounds show a very fast scintillation rise time below the resolution of the streak camera system (~10 ps) and are estimated by the fit algorithm to be close to 0 ps. All "standard" Cerium doped oxides are best described by a two component rise time fit with a significant better χ^2 value as compared to a single exponential rise time model for all tested scintillators. Interestingly the different compositions show all a similar first component of $\tau_{r1} = 0$ ps with an abundance of $R_1 \sim 83\%$ and the second component being in the order of $\tau_{r2} \sim 300$ ps with an abundance of $R_2 \sim 17\%$. This could hint that the slow second rise time component is not related to manufacturer dependent defects but likely related to a more fundamental energy transfer channel of the hot electron–hole pairs to the scintillation centers. Co-doping with divalent ions, e.g. Ca^{2+}, considerably speeds up the energy transfer in this delayed channel and consequently leads to a very fast overal scintillation rise time ~0 ps.

3.2. Oxides with 511 keV excitation

Because of the ambiguity in the exact determination of the system IRF for the X-ray excited measurements we tested all the different compositions as well with our "standard" time correlated single photon counting (TCSPC) setup with 511 keV excitation as described in Section 2.2 and in [4]. As already mentioned, with this setup it is possible to determine the IRF exactly by means of prompt (Cherenkov) emission produced in an undoped LuAG (or similar) crystal. However, in order to fullfill true single photon counting the detection efficiency of emitted scintillation photons in the stop detector has to be very low (about 0.5% of gamma interactions only lead to a stop trigger signal [4]). In order to collect enough events and sufficient statistics for the analysis long measurement times have to be accepted. A precision measurement of a crystal takes about one month, which gives high demands on the stability of the system especially on temperature [4]. Our system has proven to be temperature stable of ~0.1 °C in the period of several years [4] and is constantly monitored during data taking. The advantage

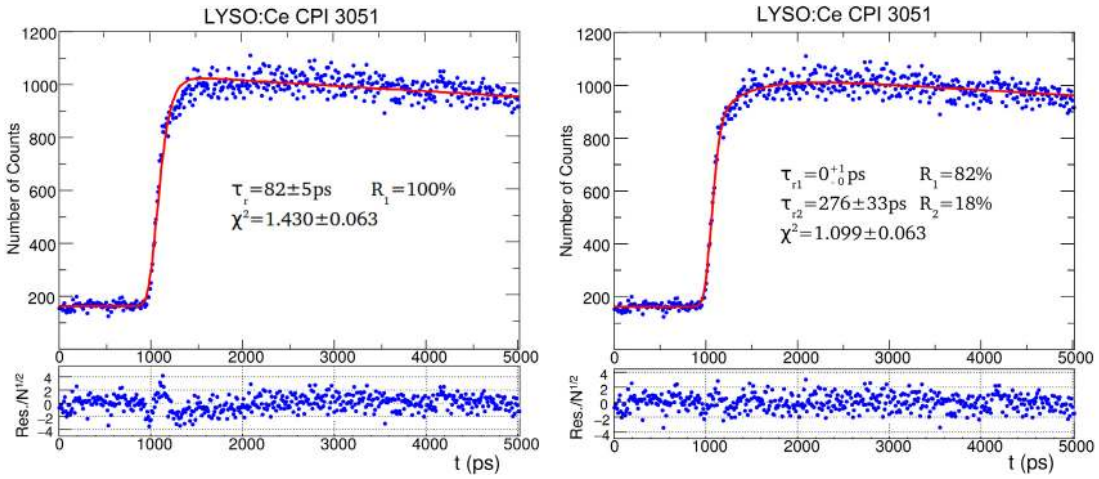

Fig. 4. Pulsed X-ray excitation. Left: Single exponential rise time fit including the full IRF of the streak camera system to the measured data for LYSO:Ce leads to an intrinsic rise time of $\tau_r = 82 \pm 5$ ps. However, modeling the intrinsic scintillation emission with only one exponential rise time still shows a high χ^2 goodness of fit value in addition to a clear peak in the residual. Right: Double exponential rise time fit including the full IRF of the streak camera system to the measured data for LYSO:Ce leads to an intrinsic rise time of $\tau_{r1} = 0^{+1}_{-0}$ ps with an abundance of $R_1 = 82\%$ and a second rise time component $\tau_{r2} = 276 \pm 33$ ps with an abundance of $R_2 = 18\%$.

Table 2
Pulsed X-ray excitation: Rise time of lutetium oxy-orthosilicates Cerium doped scintillators with and without Ca^{2+} co-doping. The statistical uncertainty for the χ^2 value is 0.063 for all measurements.

Composition	Double exponential rise					Single exponential rise		IRF [ps]
	τ_{r1} [ps]	R_1 [%]	τ_{r2} [ps]	R_2 [%]	χ^2	τ_r [ps]	χ^2	FWHM
LSO:Ce:0.2%Ca (Agile)	–	–	–	–		0	1.25	63
LSO:Ce:0.4%Ca (Agile)	–	–	–	–		0	1.09	134
LSO:Ce (CTI)	0^{+2}_{-0}	83 ± 2	296 ± 59	17 ± 2	1.11	59 ± 4	1.40	80
LSO:Ce (PML)	0^{+2}_{-0}	87 ± 2	376 ± 70	13 ± 4	1.14	53 ± 7	1.32	134
LGSO:Ce (Hitachi 1)		–	-	–		2^{+17}_{-2}	1.16	134
LYSO:Ce (CPI)	0^{+1}_{-0}	82 ± 2	276 ± 33	18 ± 3	1.10	82 ± 5	1.43	134
LYSO:Ce (Proteus)	0^{+2}_{-0}	82 ± 2	337 ± 41	18 ± 2	1.14	65 ± 6	1.35	134

Table 3
511 keV excitation: Scintillation emission decay times of the measured oxides. Most of the tested samples show a complex decay structure which can be described fairly well with two exponential decay components. For comparison the fit with only one decay component is given as well along with χ^2 values. The total number of events collected exceeds 300 000 for all crystals tested.

Composition	τ_{d1} [ns]	R_1 [%]	τ_{d2} [ns]	R_2 [%]	χ^2 (σ)	# events
LSO:Ce:0.2%Ca (Agile)	10.8 ± 1	5 ± 1	35.0 ± 0.2	95 ± 1	1.019 (0.0318)	321k
LSO:Ce:0.2%Ca (Agile)	33.1 ± 0.2	100	–	–	1.393 (0.0318)	321k
LSO:Ce:0.4%Ca (Agile)	7.5 ± 1	5 ± 1	32.4 ± 0.2	95 ± 1	1.060 (0.0318)	342k
LSO:Ce:0.4%Ca (Agile)	30.2 ± 0.2	100	–	–	1.751 (0.0318)	342k
LSO:Ce (CTI)	40.4 ± 0.2	100	–	–	1.023 (0.0318)	313k
LGSO:Ce (Hitachi 2)	11.6 ± 1	9 ± 2	37.0 ± 0.5	91 ± 2	1.085 (0.0318)	316k
LGSO:Ce (Hitachi 2)	33.4 ± 0.2	100	–	–	2.027 (0.0318)	316k
LGSO:Ce (Hitachi 1)	17.7 ± 2	8 ± 5	42 ± 1	92 ± 5	1.141 (0.0318)	654k
LGSO:Ce (Hitachi 1)	38.7 ± 0.2	100	–	–	1.757 (0.0318)	654k
LYSO:Ce (CPI)	21.5 ± 2	13 ± 5	43.8 ± 1	87 ± 5	0.955 (0.0318)	387k
LYSO:Ce (CPI)	40.0 ± 0.2	100	–	–	1.360 (0.0318)	387k
LYSO:Ce (Epic)	30.7 ± 3	39 ± 5	43 ± 1	61 ± 5	0.987 (0.0318)	269k
LYSO:Ce (Epic)	37.7 ± 0.2	100	–	–	1.147 (0.0318)	269k
LFS:Ce (Zecotek)	27.1 ± 2	19 ± 5	42 ± 1	81 ± 5	1.011 (0.0318)	357k
LFS:Ce (Zecotek)	38.7 ± 0.2	100	–	–	1.204 (0.0318)	357k

of such a low detection efficiency on the other hand is that TCSPC is as well able to measure the decay time of the scintillation emission with a time precision, defined only by the IRF, over the whole time range (gate), i.e. 1.5 μs.

Figs. 5 and 6 show examples of the scintillation emission rates measured for LSO:Ce and LYSO:Ce scintillators, respectively. It can be seen that the signal-to-noise ratio (SNR) exceeds values of a factor 1000. Such high SNR are achieved by selecting only photo-electric events in the crystal under test [4]. With these SNRs it is possible to measure the scintillation emission even in the very far tail of the decaying emission (>7τ), as can be see in Fig. 5. This precision allows to notice that for some LYSO:Ce scintillators the emission decay time is not sufficiently well described by a monoexponential function anymore, as can be seen in Fig. 6. In Table 3 the decay times extracted are summarized for the different oxides measured. Most of the times a double decay fit is more suitable with the only exception for LSO:Ce from the producer CTI. It is

Table 4
511 keV excitation: Scintillation emission rise times of the measured oxides. The co-doped scintillators show a very fast rise time in the order of 10 ps and below. Cerium doped scintillators are best described by a two component rise time fit with a very fast component <10 ps and a second component around 380 ps. For comparison the fit with only one rise time component is given as well. Shown χ^2 values are given with there associated errors in parenthesis.

Composition	Double exponential rise					Single exponential rise	
	τ_{r1} [ps]	R_1 [%]	τ_{r2} [ps]	R_2 [%]	χ^2 (σ)	τ_r [ps]	χ^2 (σ)
LSO:Ce:0.2%Ca (Agile)	–	–	–	–	–	9 ± 9	1.036 (0.0807)
LSO:Ce:0.4%Ca (Agile)	–	–	–	–	–	10 ± 10	1.074 (0.0799)
LSO:Ce (CTI)	9 ± 9	78 ± 6	306 ± 120	22 ± 6	0.994 (0.0799)	87 ± 15	1.047 (0.0799)
LGSO:Ce (Hitachi 2)	–	–	–	–	–	10 ± 10	1.155 (0.0797)
LGSO:Ce (Hitachi 1)	9 ± 9	89 ± 6	169 ± 70	11 ± 6	0.996 (0.0706)	35 ± 10	1.038 (0.0706)
LYSO:Ce (CPI)	8 ± 8	83 ± 6	304 ± 120	17 ± 6	1.007 (0.0792)	68 ± 13	1.077 (0.0792)
LYSO:Ce (Epic)	9 ± 9	80 ± 6	440 ± 177	20 ± 6	0.943 (0.0599)	77 ± 14	1.004 (0.0599)
LFS:Ce (Zecotek)	9 ± 9	77 ± 5	475 ± 180	23 ± 5	1.028 (0.0796)	90 ± 18	1.230 (0.0796)

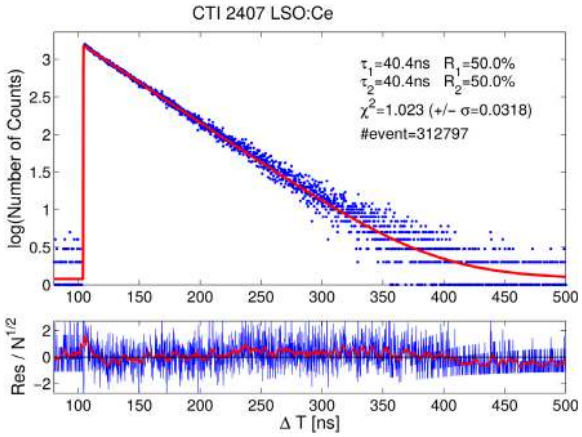

Fig. 5. 511 keV excitation: Scintillation emission decay measured for LSO:Ce from the producer CTI. Blue points represent the data with a bin width of 0.2 ns, whereas the red solid line is the fit including the IRF of the system. Only a single exponential decay of 40 ns can be observed, with no significant improvement in the quality of fit if a two decay model is applied. Note that the ordinate is the logarithm with base 10 in linear scale (semilog plot).

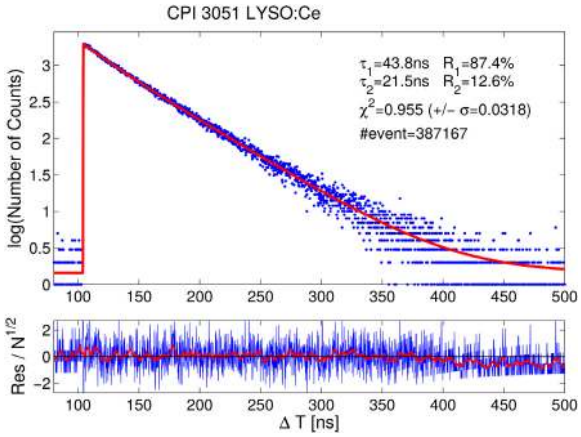

Fig. 6. 511 keV excitation: Scintillation emission decay measured for LYSO:Ce from the producer CPI. Blue points represent the data with a bin width of 0.2 ns, whereas the red solid line is the fit including the IRF of the system. In order to describe the data with sufficient accuracy a two exponential decay model is necessary with $\tau_{d1} = 21.5 \pm 2$ ns having an abundance of $R_1 = 13 \pm 5\%$ and $\tau_{d2} = 43.8 \pm 1$ ns with an abundance of $R_1 = 87 \pm 5\%$. Note that the ordinate is the logarithm with base 10 in linear scale (semilog plot).

interesting to notice that the fast decay component of LYSO and LFS is in the range of 20–30 ns with an abundance of 10%–40% and the slow component ~43 ns with an abundance of 60%–90%. On the other hand the co-doped Ca and one LGSO samples are showing a much faster decay for the slow and fast component.

Fig. 7 shows the initial scintillation emission for LSO:Ce co-doped with 0.2% Ca from the producer Agile. This crystal shows a very fast rise time with a value of $\tau_r = 9 \pm 9$ ps, being actually on the limit what our TCSPC system can resolve, hence a rise time value of zero cannot be excluded. As can be seen in Table 4 we obtain scintillation rise times $\tau_r \sim 10 \pm 10$ ps for three different compositions, i.e. LSO:Ce co-doped with 0.2%Ca (Agile), LSO:Ce co-doped with 0.4%Ca (Agile) and LGSO:Ce (Hitachi). The fact that we observe for these crystals an almost zero rise time gives confidence that the fit algorithm and determined IRF indeed is correct, as it as well includes the time smearing in the crystal due to multiple light reflection which, however, is almost negligible [4].

In Fig. 8 we show an example of a double exponential versus a single exponential rise time fit on data for LFS:Ce from the producer Zecotek. In these figures the green (wobbling) line represents a moving average of the data, in order to guide the eye. It can be seen that a double exponential rise time fit (solid red line in Fig. 8) is necessary in order to describe the data sufficiently. This finding is supported by the χ^2 value, which significantly improves if a double rise time model is used as compared to a single rise time. In Table 4 the rise time fits of the different tested composites are summarized. It can be seen that a double rise time fit is the better choice in order to describe the measured data

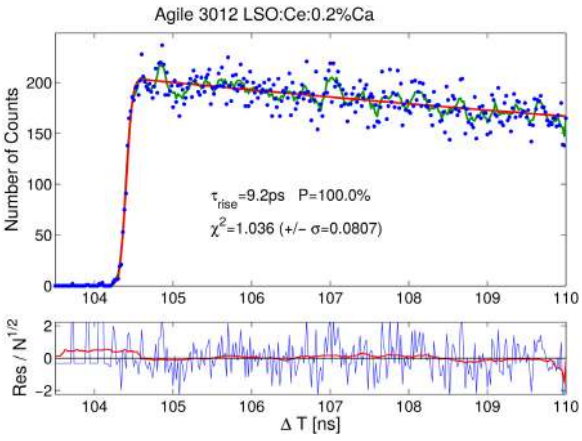

Fig. 7. 511 keV excitation: Initial scintillation emission of LSO:Ce co-doped with 0.2%Ca from the producer Agile. The red solid line represents the fit to the data including the IRF, the green solid (fluctuating) line is a moving average of the data points to guide the eye. The extracted rise time has a value of $\tau_r = 9 \pm 9$ ps, which is actually close or even below the resolution of our TCSPC setup with an IRF of 63 ps (sigma). Bin width is 20 ps.

(except for Ca^{2+} co-doped compositions), however for comparison also the single rise time fits are given.

Table 5
511 keV excitation: Scintillation decay and rise times obtained from fits to the measured emission data for the various garnet crystals. A single exponential rise time model is chosen in order to have a clear comparison between the different co-doped and non co-doped samples, revealing that co-doping with Mg^{2+} speeds up the initial emission noticeable.

Composition	Decay times					Rise times		
	τ_{d1} [ns]	R_{d1} [%]	τ_{d2} [ns]	R_{d2} [%]	χ^2 (σ)	τ_r [ps]	Camp [%]	χ^2 (σ)
GAGG:Ce	317	9	89	91	1.088 (0.026)	497	0	1.082 (0.094)
GAGG:Ce:Mg	188	34	60	66	1.291 (0.026)	72	0	0.873 (0.091)
LuAG:Ce	1784	66	97	34	1.011 (0.026)	923	0.150	1.112 (0.094)
LuAG:Ce:Mg	667	13	49	87	1.096 (0.026)	230	0.135	0.952 (0.092)
YAG:Ce	445	51	97	49	1.037 (0.026)	1560	0.080	1.132 (0.094)
YAG:Ce:Mg	134	33	51	67	1.002 (0.026)	137	0.103	1.058 (0.094)
LuAG:Pr	924	50	22	50	1.388 (0.026)	254	0.351	1.150 (0.092)

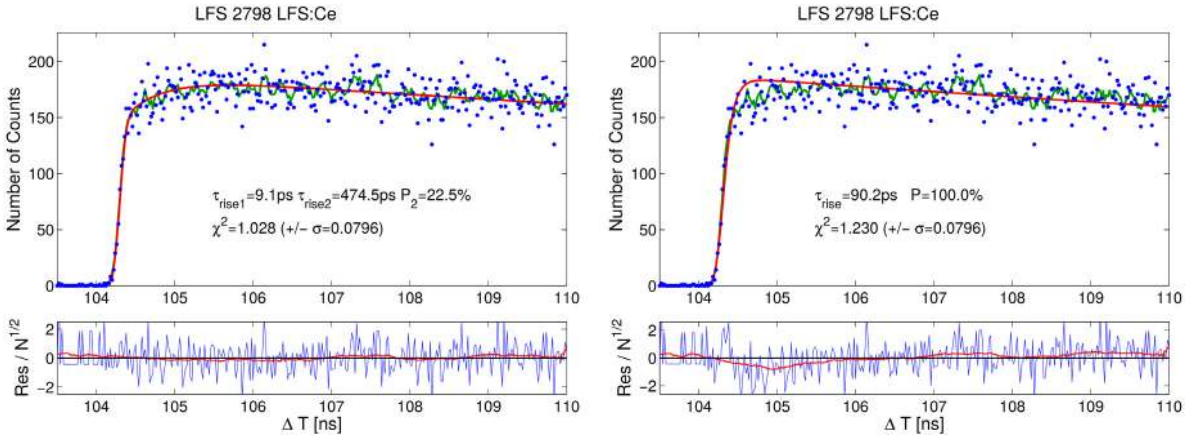

Fig. 8. 511 keV excitation: Initial scintillation emission of LFS:Ce from the producer Zecotek. Red solid line represents the fit to the data including the IRF, the green solid (fluctuating) line is a moving average of the data points to guide the eye. Only a two component rise time fit describes the measured data with sufficient accuracy. We estimate a fast component $\tau_{r1} = 9 \pm 9$ ps with an abundance of $R_1 = 77 \pm 5\%$ and a slow component of $\tau_{r2} = 475 \pm 180$ ps with an abundance of $R_1 = 23 \pm 5\%$. Using a single exponential rise time fit leads to a value of $\tau_r = 90$ ps, which is not able to fit the measured data sufficient, as can be seen on the discrepancy of data and model around 105 ns. Bin width is 20 ps.

From Table 4 it can as well be seen that apart from co-doped Ca and LGSO:Ce we consistently obtain a fast rise time component $\tau_{r1} = 9 \pm 9$ ps with an abundance of $R_1 \sim 80\%$ and a second component $\tau_{r2} \sim 380 \pm 150$ ps with an abundance of $R_2 \sim 20\%$. Both LGSO:Ce samples measured show very fast initial scintillation emissions with the older sample from Hitachi revealing two components, however, with the slow component being strongly suppressed. This gives rise to the assumption that the presence of Gadolinium in the host material or Ca^{2+} co-doping provides and additional energy transfer channel allowing for a faster population of the scintillation centers, consequently suppressing the slow rise time component seen in the other compositions. Comparing the very similar relative abundances seen for the double rise- and double decay-time fits in Tables 4 and 3 one could imagine a relation of the slow rise time component (~380 ps) with the fast decay emission (~20 ns). If this is the case possibly defects in the crystal structure could be the common base for the fast decay and slow rise times observed via trapping of electrons leading to quenching and delayed transfer. However, seeing a very similar behavior for different producers and crystals suspects a more fundamental mechanism, e.g. it could be as well possible that the two Cerium sides present in L(Y)SO interact, i.e. Ce^{4+} playing a non-negligible role in the scintillation kinematics [10].

3.3. Garnets with 511 keV excitation

Additionally to several Lutetium based oxides we as well measured the scintillation emission rates for different garnets doped with Cerium, i.e. GAGG, LuAG and YAG. Especially the effect of Mg^{2+} co-doping was studied in view of improvements in the timing performance of the various samples. In Table 5 the deconvolved scintillation decay and rise time results are summarized. Co-doping with divalent ions as Mg^{2+} improves the decay times by speeding up fast and minimizing slow components in the emission rate, which leads to an overal faster scintillation emission. We want to mention that decay time values in Table 5 are obtained using Eq. (9) to optimize the fit-parameters which might give slightly different values as reported in [5] where the more standard Eq. (8) was used for the optimization procedure. Furthermore, it can be seen that co-doping provokes a much faster scintillation rise time; improvements of a factor 10 from the nanosecond range to hundred picoseconds are observed. This finding is especially interesting for fast timing applications, where a fast rise time is beneficial [4]. This is in line with improvements observed for the oxides in the previous section.

In Fig. 9 the direct comparison of the initial scintillation emission is shown for GAGG:Ce and GAGG:Ce co-doped with Mg. It can be seen that Mg^{2+} co-doping improves the scintillation rise time noticeable from 500 to 70 ps.

Figs. 10 and 11 show the scintillation decay and rise times for LuAG:Ce and LuAG:Ce co-doped with Mg. The co-doping improves significantly the rise time and the decay time with an additional suppression of long tails in the decay emission. In both cases a pronounced prompt photon emission peak is seen at the onset of the scintillation process, as firstly reported in [4]. It should be noted that this particular LuAG:Ce sample was of lower quality, which lead to a poor decay time and as well a lower light yield. Consequently prompt photons produced, e.g. Cherenkov, are relatively to the scintillation emission more pronounced which explains the very high prompt photon peak in Fig. 10. The LuAG:Ce:Mg sample was of better quality with a higher intrinsic light yield which then provokes a relatively seen stronger scintillation emission in Fig. 11 and therefore a seemingly lower prompt photon peak.

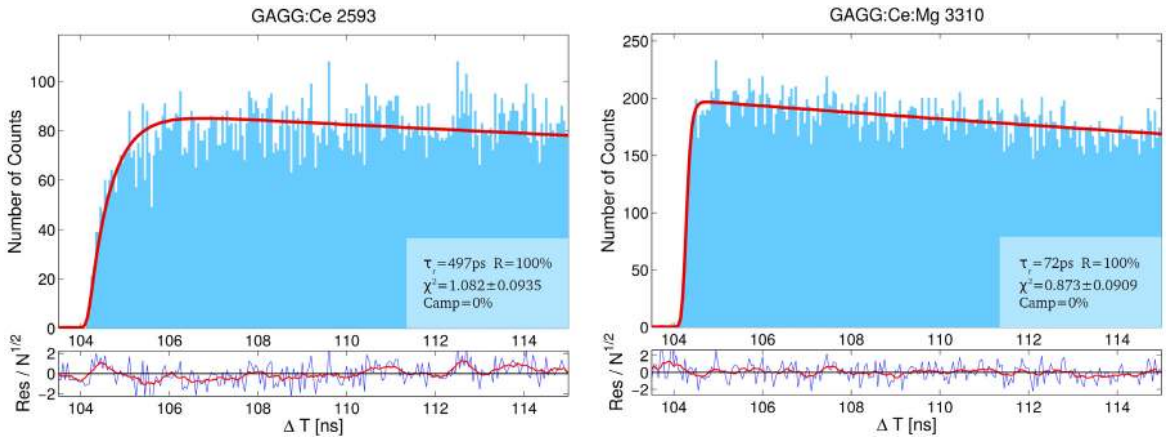

Fig. 9. 511 keV excitation: Direct comparison of Mg co-doping in GAGG:Ce. Left: Initial scintillation emission in GAGG:Ce from the producer Furukawa shows a scintillation rise time of τ_r = 497 ps. Right: Mg co-doped GAGG:Ce from the producer C&A is able to achieve a rise time of τ_r = 72 ps. Bin width is 50 ps.

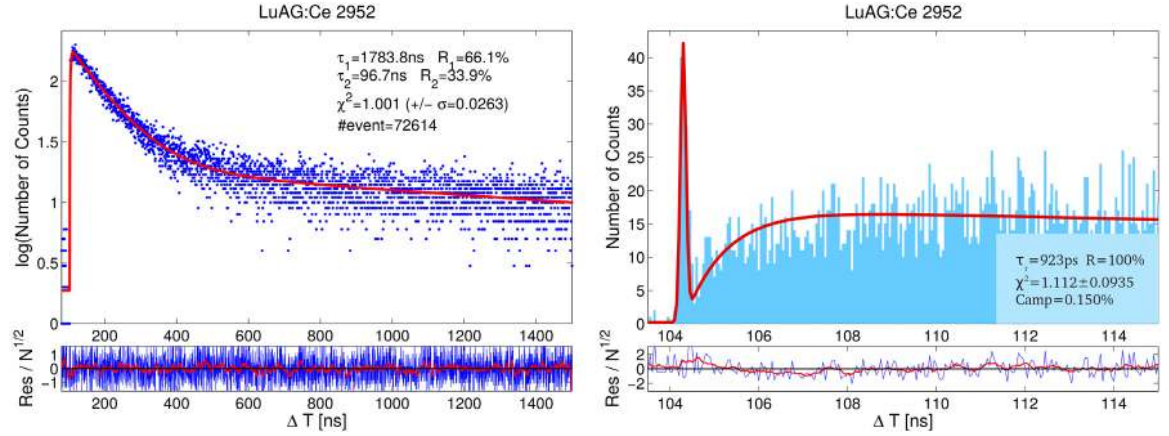

Fig. 10. 511 keV excitation. Left: Scintillation emission rate of LuAG:Ce with a 0.5 ns binning. Ordinate is the logarithm with base 10 in linear scale (semilog plot). Right: Initial scintillation emission of LuAG:Ce with a 50 ps binning. A pronounced prompt photon peak is seen at the onset of the scintillation emission, which mainly stems from Cherenkov photons produced by the hot-electron generated upon photoelectric absorption.

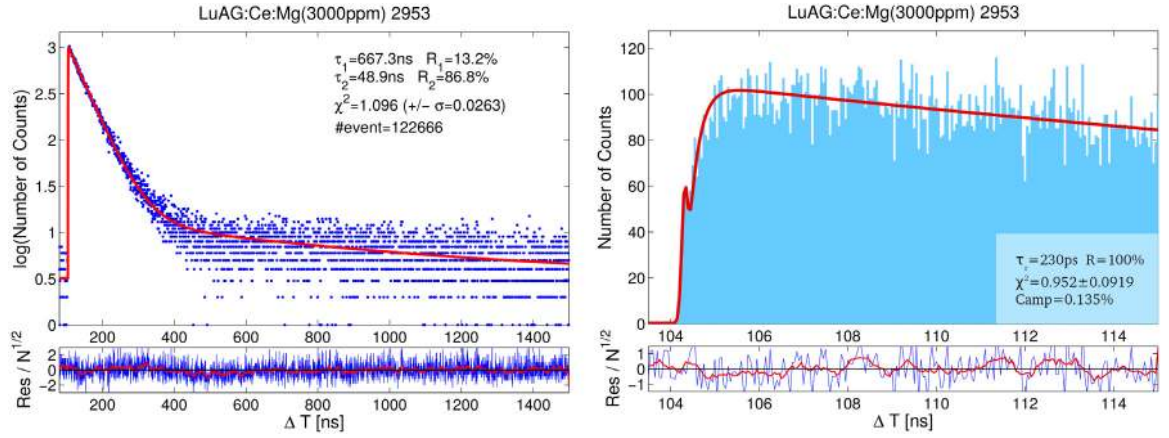

Fig. 11. 511 keV excitation. Left: Scintillation emission rate of LuAG:Ce co-doped with Mg and a 0.5 ns binning. Ordinate is the logarithm with base 10 in linear scale (semilog plot). Right: Initial scintillation emission of LuAG:Ce co-doped with Mg and a 50 ps binning. Co-doping improves the scintillation rise time noticeable as compared to the standard non co-doped scintillator.

Figs. 12 and 13 show the scintillation emission rates for YAG:Ce and YAG:Ce co-doped with Mg. Again a clearly faster scintillation decay is caused by co-doping with Mg^{2+} along an improvement in the scintillation rise time from 1560 to 137 ps. For YAG:Ce we as well observe a distinct prompt photon peak at the onset of the scintillation emission, which persists even for YAG:Ce:Mg. However, the very fast

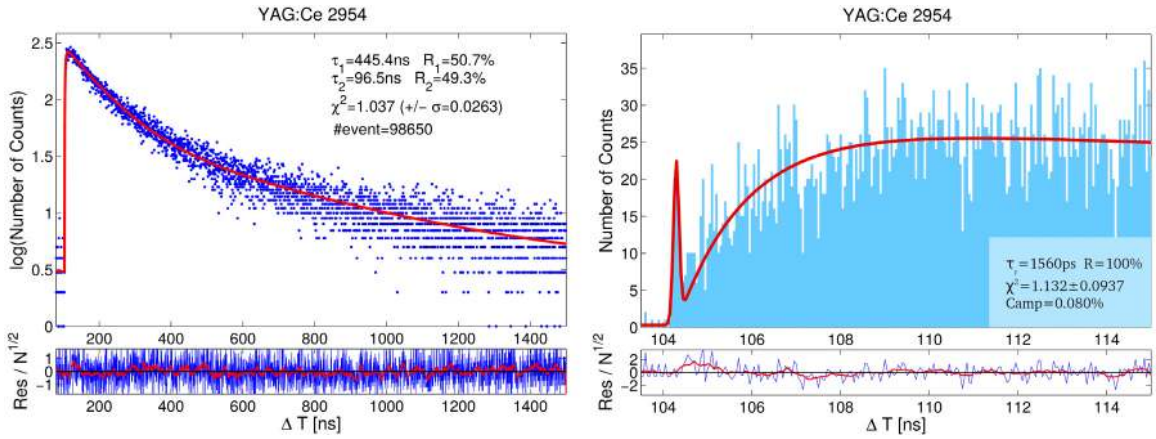

Fig. 12. 511 keV excitation. Left: Scintillation emission rate of YAG:Ce with a 0.5 ns binning. Ordinate is the logarithm with base 10 in linear scale (semilog plot). Right: Initial scintillation emission of YAG:Ce with a prompt photon peak seen at the onset of the scintillation emission. Bin width is 50 ps.

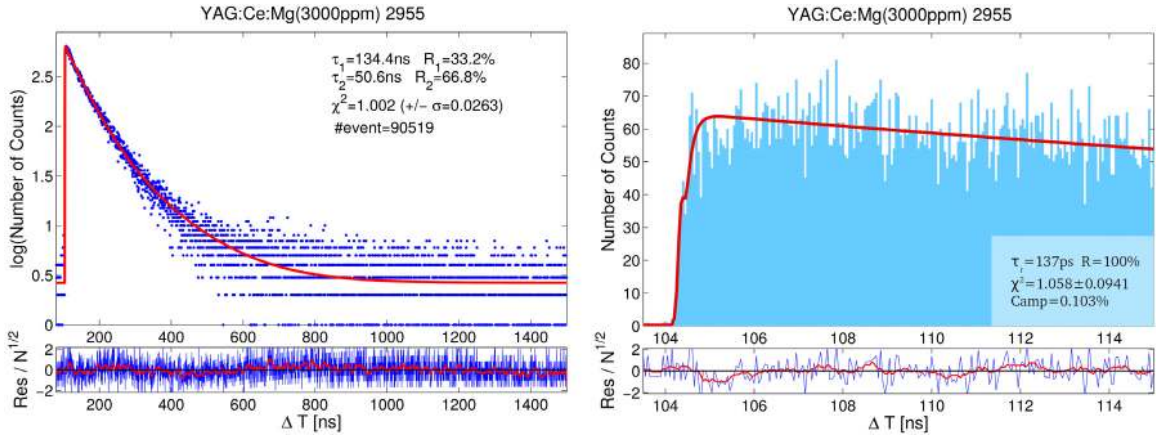

Fig. 13. 511 keV excitation. Left: Scintillation emission rate of YAG:Ce co-doped with Mg and a binning of 0.5 ns. Ordinate is the logarithm with base 10 in linear scale (semilog plot). Right: Zoom of the scintillation emission in the first 10 ns shows that co-doping improves the scintillation rise time by about a factor 10 compared to non co-doped YAG:Ce. Bin width is 50 ps.

scintillation rise time, which is in the order of the system IRF, in addition to the high light yield of YAG:Ce:Mg causes a poor separation of prompt and scintillation photons in our setup.

4. Discussion

One of the first highly time resolved X-ray induced scintillation kinematic measurements were made by Derenzo et al. [11] and have shown two components for the rise time of LYSO crystals. The first one was found to be at the level of the impulse response function of the system and below 30 ps and a second one at around 350 ps. However, there is not a follow-up study of these two rise time components with different crystals, neither a discussion regarding the origin of the slow component. More recent measurements using also X-ray excitation [12] showed only one rise time component and no significant difference between Ca^{2+} co-doped or non co-doped crystals. However, rise time measurements made using time correlated single photon counting with 511 keV gamma excitation [4] show remarkable differences between Ca^{2+} co-doped and non co-doped LSO and was as well confirmed measuring LuAG:Ce and LuAG:Pr samples, if co-doped with Ca^{2+}. As already discussed the determination of the system impulse response function is vital for extracting the rise time precisely from the measured data. In [4] Cherenkov emission in undoped LuAG crystals was used, to our knowledge, for the first time to obtain the IRF precisely and unambiguously with 511 keV excitation in a TCSPC setup. Using X-ray excitation the problem of determining the exact IRF, however, is more complicated, as the Cherenkov effect cannot be used due to the too low excitation energy of the used X-rays. Hence, one has to resort to indirect measurements or is bound to the search of very fast emitting light sources. The difficulties in determining the exact IRF for pulsed X-ray systems might be the reason why the studies reported in [12] did not see any difference between Ca^{2+} co-doped and non co-doped L(Y)SO crystals.

In the case of 511 keV excitation one has to take Cherenkov emission into account for which evidence was shown in the previous section. For LSO about 14 Cherenkov photons are produced in its transparency window [13]. This number increases to 25 for LuAG:Ce and 33 for BGO. In [14] it was estimated that for a $2 \times 2 \times 8$ mm^3 LuAG:Pr crystal about 3.4 prompt photons are sensed in the silicon photomultiplier (SiPM) photodetector with an overal detection efficiency of 11% (including losses in the crystal). This estimate is derived from the prompt to scintillation photon ratio measured to be 0.35% (see Table 5 and [4]), the measured light yield of LuAG:Pr with 21 600 photons per MeV [14] and a correction factor of 1.27 accounting for the photon detection efficiency of the used ID-Quantique single photon-detector weighted with the emission spectra of prompt (Cherenkov) and scintillation emission. Hence, in LuAG:Pr we estimate the number of prompt photons produced to be ~31, which is in line with the expected yield by Cherenkov emission solely [13]. We additionally measured this LuAG:Pr sample with X-ray excitation in our streak camera setup and did not observe prompt photon emission with the used 15 keV mean and 40 keV maximal excitation energy.

4.1. Influence of prompt photons to the fitted rise times

In Tables 2 and 4 we stated the deconvolved rise times of the tested oxides with X-ray and 511 keV excitation. The model used to estimate the scintillation rise times by fitting to Eq. (7) did not include the prompt photon term. This is a priori correct for X-ray excitation because scattered electrons do not obtain enough energy to exceed the speed of light in the crystal material. However, Cherenkov photons are produced with 511 keV excitation as the recoil electron upon photoelectric absorption has a kinetic energy of 448 keV. Thus, an average number of around 14 Cherenkov photons per 511 keV interaction are produced in L(Y)SO, which we did not account for in the fitting algorithm. This has mainly a practical reason; because of the IRF being in the same range of the rise time such an inclusion of prompt photons in the fit algorithm would create ambiguities leading to a tendency of overfitting the data, especially in the presence of a fast rise time component around 0 ps. In our former publication [4] we showed that if only a single exponential scintillation rise time model is assumed, the actual intrinsic scintillation rise time is overestimated due to the presence of prompt photons. In this work we have shown that the actual rise time of the oxides is more complex having a very fast component around 0 ps and a second component ~380 ps. In order to test the bias introduced to our fitting procedure caused by prompt photons we conducted Monte Carlo (MC) simulations generating a set of synthetic experimental data with 330k events generated (comparable to our measurement statistics), a two exponential rise time model, i.e. $\tau_{r1} = 5$ ps with $R_1 = 80\%$ and $\tau_{r2} = 300$ ps with $R_2 = 20\%$, and a variable number of prompt photons produced. On this MC generated data we applied our fitting procedure and show the fitted rise time parameters in Fig. 14. Error bars give the 99.7% confidence interval obtained by conducting 100 MC runs. It can be seen that increasing the number of prompt photons the slow rise time component $\tau_{r2} \sim 300$ ps decreases only slightly but the relative abundance of this slow rise time component R_2 decreases noticeably after a certain number of prompt photons included. This is directly related to an increase in the relative abundance of the fast $\tau_{r1} = 5$ ps rise time component $R_1 = 1 - R_2$ caused by a higher number of prompt photons at the onset of the scintillation emission. Considering the intrinsic light yield of LYSO with 20 400 photons per 511 keV [15] and 14 Cherenkov photons produced the prompt to scintillation photon ratio is 0.07% for L(Y)SO. From Fig. 14 we infer that the obtained double rise time values are negligibly biased in the case of the data presented for L(Y)SO by not taking Cherenkov emission into account in the rise time fit procedure. This conclusion is further supported by the very similar double rise times obtained with 511 keV and X-ray excitation in this work, as can be seen by comparing Tables 2 and 4.

4.2. Quality of the double-decay fits for the oxides

In Table 3 we showed that the emission for most of the L(Y,G)SO scintillators doped with Cerium are best described by a double exponential decay model. The justification of choosing a double decay model over a single decay model was given in terms of χ^2 goodness of fit values. However, in order to get a deeper understanding on the significance of using two exponential decays we evaluated the χ^2 values as a function of both decay times τ_{d1} and τ_{d2} for LYSO:Ce from the producer CPI, which can be seen in Fig. 15. The shown χ^2-values are calculated using Eq. (8) with all remaining parameters fitted in order to minimize the χ^2 according to Eq. (9). It can be seen that a double exponential decay model is indispensable, however, the range of acceptable decay times is rather large, ranging from 10 to 30 ns for the fast decay component and 42 to 50 ns for the slow decay component. As already mentioned the detection efficiency of our TCSPC setup is ~0.5% and therefore we do not suspect a noticeable bias due to multiple photon counting. This is corroborated by the fact that the scintillation emission rate of LSO:Ce from CTI does not show a similar behavior and is sufficiently well described by a single exponential fit only.

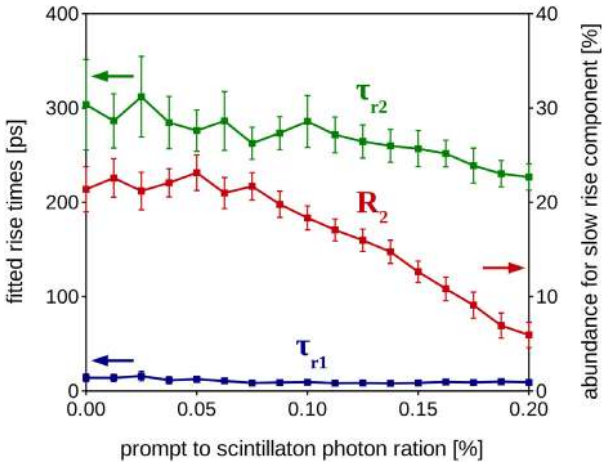

Fig. 14. Fitted rise times versus the ratio of prompt to scintillation photons for MC generated data with $\tau_{r1} = 5$ ps, $R_1 = 80\%$ and $\tau_{r2} = 300$ ps, $R_2 = 20\%$ as input parameters. Increasing the prompt to scintillation photon ratio leads to a fitted lower abundance of the slow rise time component R_2 and slightly lower rise time value τ_{r2}, whereas τ_{r1} stays basically unchanged below the intrinsic resolution of our system.

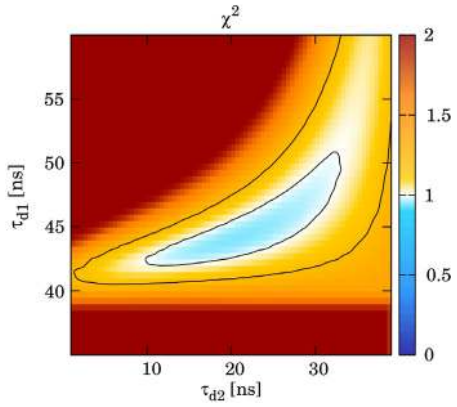

Fig. 15. χ^2 as a function of τ_{d1} and τ_{d2} for LYSO:Ce from the producer CPI. The relative abundances R_1 and R_2 are chosen to give the minimum χ^2 value for each decays. The best fit is obtained with $\tau_{d2} = 21.5$ ns and $\tau_{d1} = 44$ ns.

4.3. Outlook: timing using prompt photons in TOF-PET

Prompt photon emission in scintillators has the potential to significantly improve the coincidence time resolution in time of flight positron emission tomography. As already mentioned a CTR of 20 ps FWHM and higher can change several limiting aspects of PET drastically with new possibilities in PET diagnostics, pharmaceutical research or dose monitoring for proton therapy. In order to study the theoretical CTR improvement due to prompt photons we used Cramér–Rao lower bound calculations as described in [16]. Results are shown in Fig. 16, where the solid lines show the necessary single photon time resolution (SPTR) and photon detection efficiency (PDE) in order to reach a CTR of 20 ps for the case of 10, 20, 30, 100 and 500 prompt photons produced at the onset of the standard LYSO:Ce scintillation emission. Parameters for LYSO:Ce used are: $\tau_{r1} = 9$ ps with 78% abundance, $\tau_{r2} = 306$ ps with 22% abundance, $\tau_d = 41$ ns and an intrinsic light yield of 40 kph/MeV. These lower bound calculations include the additional photon transport time spread (PTS) and light transfer efficiency (LTE) or loss in a $2 \times 2 \times 3$ mm^3 crystal. It can be seen that theoretically 30 prompt photons produced, as in the case of LuAG:Pr, could be already enough to reach a CTR of 20 ps FWHM, if the SPTR of the photodetector reaches

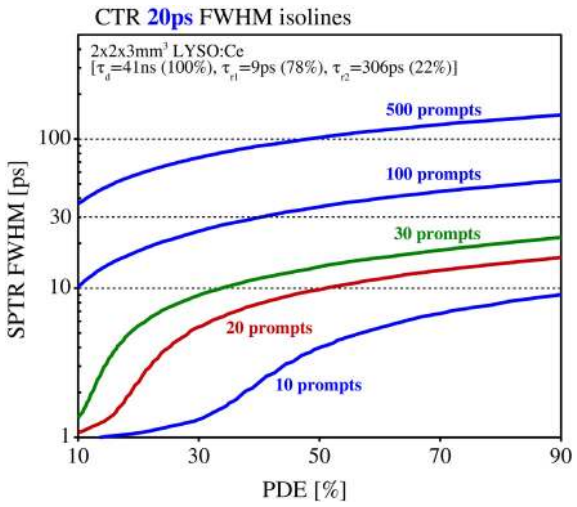

Fig. 16. CTR isolines showing SPTR and PDE values on the axis in order to reach 20 ps FWHM for the case of 10 to 500 prompt photons produced.

values of close to 10 ps FWHM and a PDE of higher 50%. These values are indeed possible to achieve as shown in [17,14]. The challenge will be to develop photodetectors with such high SPTR and PDE for larger sizes with at least 1×1 mm ^{2}. The production of more prompt photons would relax the needs imposed on the photodetector and would as well allow for longer crystals. Such sources of prompt photons could for example be hot-intraband luminescence [18,19] and/or quantum confined nanocrystals [20,21].

5. Conclusion

We have measured the scintillation kinematics under 511 keV and X-ray excitation of various inorganic scintillators, i.e. LSO, LYSO, LGSO, LFS, LuAG, YAG and GAGG, doped with Cerium and selected co-doped with Calcium or Magnesium. For L(Y)SO:Ce crystals we observed two exponential rise times, one below the intrinsic resolution of our setup (i.e. <10 ps) and the second being in the order of 380 ps. Co-doping LSO:Ce with Ca^{2+} suppresses this slow component completely leading to an overal rise time below 10 ps, which was as well observed for LGSO:Ce crystals. These results were obtained equally under X-ray and 511 keV excitation, following a proper evaluation of the two setup's impulse response functions. A similar speeding up of the scintillation rise time we see in LuAG:Ce, YAG:Ce and GAGG:Ce crystals when co-doped with Mg^{2+}. Further tests are planned and ongoing to investigate the temperature dependence of both rise time components in order to understand their precise origin. In the garnet crystals we additionally are able to identify a prompt photon peak at the onset of the scintillation process, which most likely stems from Cherenkov radiation. Harvesting these prompt photons for highest time resolution in PET can open new doors to achieve sub-20 ps timing with state-of-the-art photodetectors showing highest SPTR and PDE.

Acknowledgments

This work has been performed in the framework of the Crystal Clear Collaboration and received funding from the European advanced ERC grant TICAL 338953 (PI P. Lecoq).

References

[1] S. Gundacker, Time Resolution in Scintillator Bbased Ddetectors for Positron Emission Tomography (Ph.D. thesis), Vienna University of Technology, 2014.
[2] R. Post, L. Schiff, Statistical limitations on the resolving time of a scintillation counter, Phys. Rev. 80 (6) (1950) 1113.
[3] P. Lecoq, M. Korzhik, A. Vasiliev, Can Transient phenomena help improving time resolution in scintillators? IEEE Trans. Nucl. Sci. 61 (1) (2014) 229–234.
[4] S. Gundacker, E. Auffray, K. Pauwels, P. Lecoq, Measurement of intrinsic rise times for various L(Y)SO and LuAG scintillators with a general study of prompt photons to achieve 10ps in TOF-PET, IOP Phys. Med. Biol. 61 (2016) 2802–2837.
[5] M. Lucchini, S. Gundacker, P. Lecoq, A. Benaglia, M. Nikl, K. Kamada, A. Yoshikawa, E. Auffray, Timing capabilities of garnet crystals for detection of high energy charged particles, Nucl. Instrum. Methods Phys. Res. A 852 (2017) 1–9.
[6] S. Gundacker, E. Auffray, B. Frisch, T. Meyer, P. Jarron, P. Lecoq, SiPM photodetectors for highest time resolution in PET, in: Proceedings of Science PoS(PhotoDet 2012)016, LAL Orsay, France, 2012.
[7] Hamamatsu K.K., private communication, 2014.
[8] R.M. Turtos, Prompt Photon Emission - A Novel Approach Towards Highest Time Resolution with Scintillators (Ph.D. thesis), University Degli Studi Di Milano-Bicocca, 2017.
[9] W. Eadie, D. Drijard, F. James, M. Roos, B. Sadoulet, Statistical Methods in Experimental Physics, North-Holland, 1971.
[10] S. Blahuta, A. Bessière, B. Viana, P. Dorenbos, V. Ouspenski, Evidence and consequences of Ce^{4+} in LYSO:Ce,Ca and LYSO:Ce,Mg single crystals for medical imaging applications, IEEE Trans. Nucl. Sci. 60 (4) (2013) 3134–3141.
[11] S. Derenzo, M. Weber, W. Moses, C. Dujardin, Measurement of the intrinsic rise times of common inorganic scintillators, IEEE Trans. Nucl. Sci. 47 (3) (2000) 860–864.
[12] D.N. ter Weele, D.R. Schaart, P. Dorenbos, Intrinsic scintillation pulse shape measurements by means of picosecond x-ray excitation for fast timing applications, Nucl. Instrum. Methods Phys. Res. A 767 (2014) 206–211.
[13] S.E. Brunner, L. Gruber, J. Marton, K. Suzuki, A. Hirtl, Studies on the cherenkov effect for improved time resolution of TOF-PET, IEEE Trans. Nucl. Sci. 61 (1) (2014) 443–447.
[14] S. Gundacker, F. Acerbi, E. Auffray, A. Gola, M. Nemallapudi, G. Paternoster, C. Piemonte, P. Lecoq, State of the art timing in TOF-PET detectors with LuAG, GAGG and L(Y)SO scintillators of various sizes coupled to FBK-SiPMs, Jinst, P08008, JINST 11 P08008, 2016.
[15] R. Turtos, S. Gundacker, M. Pizzichemi, A. Ghezzi, K. Pauwels, E. Auffray, P. Lecoq, M. Paganoni, Measurement of LYSO intrinsic light yield using electron excitation, IEEE Trans. Nucl. Sci. 63 (2) (2016) 475–479.
[16] S. Seifert, H.T. van Dam, D.R. Schaart, The lower bound on the timing resolution of scintillation detectors, Phys. Med. Biol. 57 (2012) 1797–1814.
[17] M. Nemallapudi, S. Gundacker, P. Lecoq, E. Auffray, Single photon time resolution of state of the art SiPMs, Jinst, P10016, JINST 11 P10016, 2016.
[18] S. Omelkov, V. Nagirnyi, A. Vasilev, M. Kirm, New features of hot intraband luminescence for fast timing, J. Lumin. 176 (2016) 309–317.
[19] P. Lecoq, Development of new scintillators for medical applications, Nucl. Instrum. Methods (2015). http://dx.doi.org/10.1016/j.nima.2015.08.041.
[20] R.M. Turtos, S. Gundacker, M.T. Lucchini, L. Procházková, V. Cuba, H. Buresová, J. Mrázek, M. Nikl, P. Lecoq, E. Auffray, Timing performance of ZnO:Ga nanopowder composite scintillators, Phys. Status Solidi RRL 10 (11) (2016) 843–847.
[21] R. Turtos, S. Gundacker, A. Polovitsyn, S. Christodoulou, M. Salomoni, E. Auffray, P.L.I. Moreels, J. Grim, Ultrafast emission from colloidal nanocrystals under pulsed X-ray excitation, JINST, P10015, JINST 11 P10015, 2016.